

# Structural Basis of Conserved Cysteine in the Fibroblast Growth Factor Family: Evidence for a Vestigial Half-Cystine

Jihun Lee and Michael Blaber\*

Department of Biomedical Sciences, College of Medicine, Florida State University, Tallahassee, FL 32306-4300, USA

Received 8 June 2009;  
received in revised form 31 July 2009;  
accepted 6 August 2009  
Available online 13 August 2009

The 22 members of the mouse/human fibroblast growth factor (FGF) family of proteins contain a conserved cysteine residue at position 83 (numbering scheme of the 140-residue form of FGF-1). Sequence and structure information suggests that this position is a free cysteine in 16 members and participates as a half-cystine in at least 3 (and perhaps as many as 6) other members. While a structural role as a half-cystine provides a stability basis for possible selective pressure, it is less clear why this residue is conserved as a free cysteine (although free buried thiols can limit protein functional half-life). To probe the structural role of the free cysteine at position 83 in FGF-1, we constructed Ala, Ser, Thr, Val, and Ile mutations and determined their effects on structure and stability. These results show that position 83 in FGF-1 is thermodynamically optimized to accept a free cysteine. A second cysteine mutation was introduced into wild-type FGF-1 at adjacent position Ala66, which is known to participate as a half-cystine with position 83 in FGF-8, FGF-19, and FGF-23. Results show that, unlike position 83, a free cysteine at position 66 destabilizes FGF-1; however, upon oxidation, a near-optimal disulfide bond is formed between Cys66 and Cys83, resulting in ~14 kJ/mol of increased thermostability. Thus, while the conserved free cysteine at position 83 in the majority of the FGF proteins may have a principal role in limiting functional half-life, evidence suggests that it is a vestigial half-cystine.

© 2009 Elsevier Ltd. All rights reserved.

**Keywords:** fibroblast growth factor-1; protein engineering; disulfide bond; half-cystine; protein evolution

Edited by R. Huber

## Introduction

Fibroblast growth factors (FGFs) (gene, *Fgf*; protein, FGF) are a family of polypeptides with diverse roles in development and metabolism. *Fgfs* have been found in multicellular organisms ranging from *Caenorhabditis elegans* to *Homo sapiens*; two *Fgf* genes have been identified in *C. elegans*, while mouse and human each share 22 *Fgf* genes. The evolutionary expansion of the *Fgf* family correlates with the evolution of metazoa to vertebrates and is hypothesized to have occurred in two main phases,<sup>1,2</sup> reflecting the “2R hypothesis” of vertebrate evolution.<sup>3</sup> The first phase, during early metazoan evolution, is pro-

posed to have involved expansion of one or a few *Fgf* members into seven distinct *Fgf* subfamilies; a subsequent second phase of expansion, during the evolution of early vertebrates, resulted in the generation of approximately three members per subfamily, leading to the 22 extant *Fgfs* within mouse and human.<sup>2,4</sup>

The fundamental FGF protein structure is described by an ~120-amino-acid domain that forms a  $\beta$ -trefoil architecture.<sup>5</sup> Among the 22 members of the human FGF family, three positions are absolutely conserved and include Gly71, Cys83, and Phe132 (numbering scheme of the 140-amino-acid form of FGF-1). Gly71 is located at the *i*+3 position in a type 1  $\beta$ -turn and is the statistically preferred residue at this position due to structural considerations of backbone strain.<sup>6–9</sup> Phe132 is a large aromatic residue that forms part of the hydrophobic core of the protein. Such large hydrophobic residues within the protein interior make a substantial contribution

\*Corresponding author. E-mail address:

michael.blaber@med.fsu.edu.

Abbreviations used: FGF, fibroblast growth factor; PDB, Protein Data Bank.

to protein stability.<sup>10–12</sup> Cys83 is located at a solvent-inaccessible position in the protein and, therefore, has no identifiable role related to receptor binding functionality, neither does it provide a significant buried hydrophobic area that might contribute to stability. As sequence information for the FGF proteins emerged and as the conserved nature of Cys83 became apparent, it was believed that this cysteine likely formed one-half of a disulfide bond and therefore played a key role in stabilizing the FGF structure.<sup>13,14</sup> In the case of FGF-1, it was later shown that Cys83 was not involved in a disulfide bond and was present in the structure as a buried free cysteine.<sup>15</sup> Subsequent X-ray structure determinations proved that Cys83 is a free thiol in FGF-1,<sup>16</sup> FGF-2,<sup>17</sup> FGF-4,<sup>18</sup> FGF-7,<sup>19</sup> FGF-9,<sup>20</sup> FGF-10,<sup>21</sup> and FGF-12.<sup>22</sup> However, FGF-8, FGF-17, FGF-18, FGF-19, FGF-21, and FGF-23 each contain a cysteine residue at position 66 that lies adjacent to position 83. The crystal structures of FGF-8,<sup>22</sup> FGF-19,<sup>23</sup> and FGF-23<sup>24</sup> have been solved, and each shows a disulfide bond formed between Cys83 and the adjacent Cys66.

Among the group of FGFs that have a cysteine at position 66, FGF-8, FGF-17, and FGF-18 constitute the *Fgf8* subfamily, and FGF-19, FGF-21, and FGF-23 constitute the *hFgf* (endocrine-like) subfamily.<sup>2,25</sup> Thus, a disulfide bond involving positions 66 and 83 appears to be a potentially ancient structural feature of the FGF family, although an overwhelming majority of the extant FGF family members have a free cysteine at position 83. The contribution of a disulfide bond to the thermostability of the *Fgf8* and *hFgf* subfamilies provides a structural rationale for the conservation of a cysteine at position 83; however, it is unclear what the selective pressure might be to retain a free cysteine at position 83 in the majority of the FGF proteins.

To better understand the basis for the absolute conservation of Cys83 in the FGF family, particularly when present as a free cysteine, we characterized the X-ray structures and thermodynamic properties of Thr, Ser, Ala, Val, and Ile point mutations at position 83 in FGF-1 (which, along with FGF-2, constitute the *Fgf1* subfamily). Thermodynamic data show that Cys is the only residue that can be accommodated at position 83 without causing significant destabilization. X-ray data indicate that the structural environment surrounding Cys83 is essentially rigid and unable to adapt to even small changes that might otherwise accommodate alternative amino acids. Furthermore, structural data show that the buried free cysteine at position 83 in FGF-1 participates as a rare H-bond acceptor, suggesting that the cysteine may be partially deprotonated and, therefore, may be a reactive thiol. Prior studies have demonstrated a role for buried thiol reactivity in limiting the functional half-life of FGF-1.<sup>26,27</sup>

The introduction of a cysteine mutation at adjacent position 66, which in members of two of the seven *Fgf* subfamilies forms a disulfide with position 83, results in a form of FGF-1 that is less stable than wild type under reducing conditions but

substantially more stable than wild type under oxidizing conditions, with concomitant formation of an intramolecular disulfide bond. The results suggest, therefore, that although a cysteine residue is conserved at position 83 in all members of the *Fgf* family of proteins, there are two distinctly different functional roles for this cysteine, depending upon the particular FGF protein. For members where adjacent position 66 is a cysteine, position 83 can readily form an intramolecular disulfide bond that provides significant thermodynamic stability. For other FGF members where Cys83 is present as a buried free cysteine, even though a cysteine may be the most structurally preferred residue at this position, thiol reactivity can contribute to an irreversible unfolding pathway that can effectively regulate the protein functional half-life.<sup>26,27,28</sup>

## Results

### Mutant protein purification

All mutant proteins, except for Cys83→Ile and Ala66→Cys mutations, purified with equivalent yield (~20 mg/L) and purity (i.e., homogenous by Coomassie-Blue-stained SDS-PAGE) as with the wild-type recombinant protein. The Cys83→Ile mutation exhibited a very low solubility, resulting in substantial precipitation during purification; however, when constructed in the stabilizing Lys12→Val/Cys117→Val mutant background,<sup>29</sup> the Cys83→Ile/Lys12→Val/Cys117→Val mutant purified with a yield of ~15 mg/L soluble protein. The Ala66→Cys mutation, purified with no DTT in purification buffers, yielded a doublet band on nonreducing SDS-PAGE of varying ratios depending on the preparation (data not shown). One band in this doublet migrated equivalent to wild-type FGF-1, and the other (typically the more intense of the two bands) was a faster-migrating species. This faster-migrating species subsequently resolved identical with wild-type FGF-1 upon reduction, indicating the presence of an intramolecular disulfide bond. Essentially homogenous preparations of this putative disulfide-bonded form could be obtained after extensive air incubation of the purified sample. Homogenous preparations of a reduced form of the Ala66→Cys mutant protein were readily obtained by the inclusion of 10 mM DTT in all buffer components utilized throughout the purification.

### Isothermal equilibrium denaturation

The derived thermodynamic parameters for all mutant proteins, in comparison to wild-type FGF-1 (or Lys12→Val/Cys117→Val reference mutant), are summarized in Table 1. All of the point mutations at position 83 destabilize the protein and vary from 5.2 to 12.6 kJ/mol.  $\Delta\Delta G$  for the Cys83→Ser mutation is 6.8 kJ/mol, in good agreement with our

**Table 1.** Thermodynamic parameters for FGF-1 mutants in crystallization buffer, as determined by isothermal equilibrium denaturation using guanidine hydrochloride and as monitored by fluorescence spectroscopy

Protein	$\Delta G$ (kJ/mol)	$m$ -value (kJ/mol M)	$C_m$ (M)	$\Delta\Delta G^a$ (kJ/mol)
Wild type	26.6±0.9	20.3±0.7	1.29±0.01	—
Lys12→Val/Cys117→Val	33.9±0.4	20.0±0.2	1.69±0.01	-8.1
Cys83→Ala	20.8±0.7	20.5±0.3	1.01±0.02	5.7
Cys83→Ser	20.0±0.8	20.9±0.7	0.96±0.01	6.9
Cys83→Thr	20.5±0.9	19.8±0.6	1.03±0.02	5.2
Cys83→Val	14.7±0.5	20.9±0.7	0.70±0.01	12.1
Cys83→Ile/Lys12→Val/Cys117→Val	20.9±0.4	19.7±0.4	1.06±0.02	12.6 <sup>b</sup>
Ala66→Cys (reduced)	16.4±0.2	16.3±0.1	1.01±0.01	5.1
Ala66→Cys (oxidized)	30.5±1.9	16.6±1.0	1.84±0.01	-10.2 (-13.7 <sup>c</sup> )

<sup>a</sup>  $\Delta\Delta G = (C_m^{WT} - C_m^{mutant})(m_{WT} + m_{mutant})/2$ , as described by Pace and Scholtz.<sup>50</sup> A negative value of  $\Delta\Delta G$  indicates a more stable mutation, and error is stated as the standard error from multiple data sets.

<sup>b</sup>  $\Delta\Delta G$  value calculated with respect to the background mutant Lys12→Val/Cys117→Val.

<sup>c</sup>  $\Delta\Delta G$  value calculated with respect to the reduced form of A66C.

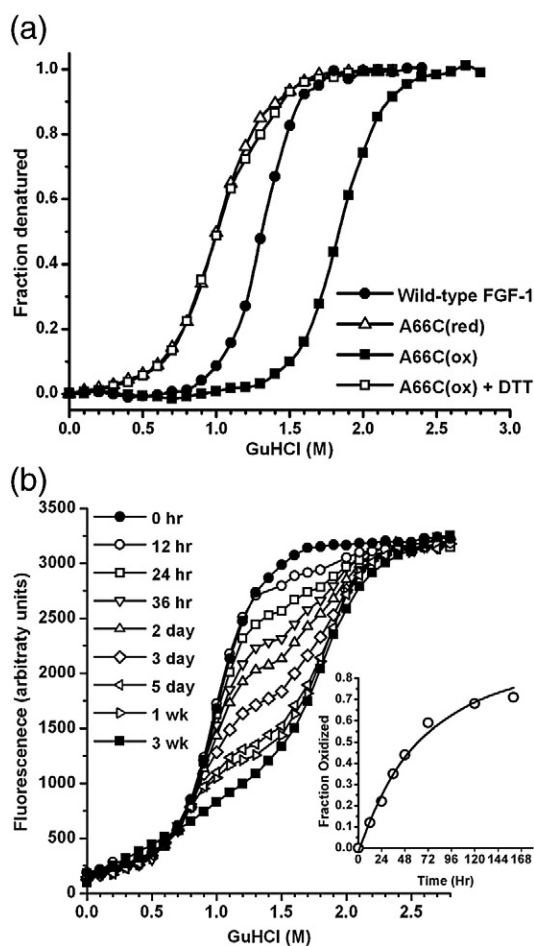


**Fig. 1.** (a) Isothermal equilibrium denaturation profiles (normalized to fraction denatured) for wild-type FGF-1; Ala66→Cys mutant purified in the presence of 10 mM DTT (red); Ala66→Cys purified in the absence of 10 mM DTT (ox); and Ala66→Cys purified in the absence of 10 mM DTT and subsequently reduced by the addition of 10 mM DTT (ox+DTT). (b) Isothermal equilibrium denaturation data (raw fluorescence data) for an air oxidation time course of the Ala66→Cys FGF-1 mutant (initially purified under reducing conditions). The inset shows a progress curve for the fractional increase in the Ala66→Cys oxidized form from the isothermal equilibrium data (yielding a corresponding decay half-life of the reduced form of 60 h).

previous report.<sup>26</sup> All proteins exhibited excellent agreement with a two-state denaturation model. The fully oxidized form of the Ala66→Cys mutant was 10.2 kJ/mol more stable than the wild-type protein, while the fully reduced form was 5.1 kJ/mol less stable than the wild-type protein; furthermore, upon addition of 10 mM DTT, the isothermal equilibrium denaturation profile of the fully oxidized form reverted to the profile of the fully reduced form (Fig. 1a). Air oxidation of an initially reduced form of the Ala66→Cys mutation exhibited evidence of both oxidized and reduced components in the denaturation profile, and the relative mole fraction of the oxidized component was directly proportional to the extent of incubation (Fig. 1b). Under air oxidation, the reduced Ala66→Cys mutant protein converted into the more stable oxidized form with an apparent first-order exponential decay kinetic rate constant of 60 h (Fig. 1b, inset).

### Mass spectrometry

Mass spectrometry of a trypsin digest of the Ala66→Cys protein, prepared under both reducing and oxidizing conditions, identified mass fragments of 3513.74 and 3511.42 Da, respectively. These fragments correspond to amino acid residue positions 58–88 and include both Cys66 and Cys83 residues. If these two residues are present as a disulfide-bonded cystine, this peptide will have a mass that is 2 Da lighter than if they are present as individual protonated free cysteines. The expected mass of the reduced free-cysteine form is 3514 Da, and that of the oxidized cystine form is 3512 Da. These masses are in agreement with mass spectrometry data and indicate that, when purified in the absence of DTT, the majority of the protein contains a disulfide-bonded cystine residue involving positions Cys66 and Cys83.

### X-ray structure determination

Diffraction-quality crystals were obtained for Cys83→Ser, Cys83→Thr, Cys83→Ala, Cys83→Val, and Cys83→Ile/Lys12→Val/Cys117→Val,

and for the reduced and oxidized forms of the Ala66→Cys mutant proteins. X-ray diffraction data sets with resolution ranges between 1.90 and 2.55 Å were collected with substantial completion in each case, and all structures were refined to acceptable crystallographic residual and stereochemistry (Table 2). All mutants, except for Cys83→Ile/Lys12→Val/Cys117→Val and reduced Ala66→Cys, crystallized in orthorhombic space group (C222<sub>1</sub>) with two molecules in the asymmetric unit (isomorphous with the wild-type FGF-1 crystal form). The Cys83→Ile/Lys12→Val/Cys117→Val and reduced Ala66→Cys mutant proteins both crystallized in a novel P2<sub>1</sub> monoclinic space group. Analysis of this P2<sub>1</sub> cell indicated a Matthews coefficient of ~2.8 Å<sup>3</sup>/Da, with four molecules in the asymmetric unit. These four molecules were successfully positioned using molecular replacement, with wild-type FGF-1 [Protein Data Bank (PDB) code 1JQZ] as search model in both cases. The 2F<sub>o</sub> - F<sub>c</sub> difference electron density was unambiguous at the mutation site(s), and mutant structures could be accurately modeled in each case. A summary of the individual X-ray structures is provided below (the side chain of solvent-exposed residue Glu81 adopts various conformations in position 83 mutant structures, but this appears to be due to local crystal contact and not due to position 83 mutations).

#### Cys83→Ala

The wild-type Cys83 S<sup>γ</sup> participates as an H-bond acceptor with the main-chain amide of residue Asn80 and with an H-bond distance of 3.5 Å. The

Ala mutation deletes the side-chain S<sup>γ</sup> group and the associated H-bond with the Asn80 main-chain amide (Fig. 2a). The structure of the Ala mutation shows no obvious H-bond partner for the Asn80 main-chain amide, and it therefore appears as an unsatisfied H-bond group. There is minimal structural collapse in response to the deletion of the side-chain S<sup>γ</sup> group, and cavity calculation indicates the presence of a novel 7-Å<sup>3</sup> cavity (detected using a 1.0-Å-radius probe) adjacent to C<sup>β</sup> at the former location of the S<sup>γ</sup>.

#### Cys83→Ser

The Ser mutation substitutes an O<sup>γ</sup> hydroxyl for wild-type Cys S<sup>γ</sup>. The mutant Ser side chain adopts the same rotamer (*gauche+*) as the wild-type Cys and is thus oriented appropriately to participate as an H-bond acceptor to the Asn80 main-chain amide (Fig. 2b). Due to the smaller diameter of the oxygen atom, the structure must collapse somewhat to bring the Asn80 main-chain amide within effective H-bond distance of the mutant Ser83 O<sup>γ</sup>. However, the mutant structure shows minimal evidence of any such structural adjustment, and the resulting Ser83 O<sup>γ</sup> and Asn80 N atomic distance is 3.7±0.4 Å (average of two independent molecules in the asymmetric unit), indicating that no significant H-bond interaction occurs between these groups. The most pronounced structural change in the Ser mutant is a 20° rotation of the Asn80 χ<sub>2</sub> angle, resulting in a novel H-bond interaction (2.7 Å) between the introduced Ser83 O<sup>γ</sup> and Asn80 O<sup>δ1</sup>. In this H-bond interaction, the Ser83 O<sup>γ</sup> is the *donor* to the Asn80

**Table 2.** Crystallographic data collection and refinement statistics (values in parentheses are for the highest-resolution shell)

	Cys83→Ala	Cys83→Ser	Cys83→Thr	Cys83→Val	Cys83→Ile/ Lys12→Val/ Cys117→Val	Ala66→Cys (reduced)	Ala66→Cys (oxidized)
Space group	C222 <sub>1</sub>	C222 <sub>1</sub>	C222 <sub>1</sub>	C222 <sub>1</sub>	P2 <sub>1</sub>	P2 <sub>1</sub>	C222 <sub>1</sub>
Unit cell parameters <i>a</i> , <i>b</i> , <i>c</i> (Å)	74.4, 95.4, 108.9	75.4, 94.4, 108.7	74.2, 95.9, 109.1	74.7, 97.4, 108.2	50.8, 108.1, 67.7	51.4, 110.8, 67.3	74.0, 96.9, 108.9
Unit cell parameter β (°)					103.7	105.3	
Maximum resolution (Å)	1.90	2.10	1.90	1.90	2.55	2.15	2.30
Mosaicity (°)	1.1	0.5	1.0	0.6	1.3	1.2	1.4
Redundancy	10.2	10.1	11.7	12.8	3.6	3.4	6.8
Molecules per asymmetric unit	2	2	2	2	4	4	2
Matthews coefficient (Å <sup>3</sup> /Da)	2.93	2.93	2.94	2.98	2.73	2.80	2.96
Total reflections	311,775	231,997	354,786	396,203	79,101	133,744	103,847
Unique reflections	30,504	22,991	30,327	31,013	21,754	39,339	15,240
<i>I</i> / <i>σ</i>	30.6 (3.0)	37.1 (6.8)	48.3 (7.5)	58.5 (6.0)	6.0 (3.0)	18.0 (3.1)	24.8 (3.3)
Completion (%)	98.2 (85.2)	100 (100)	97.4 (90.9)	98.5 (84.8)	94.8 (93.1)	99.7 (100)	85.7 (84.4)
<i>R</i> <sub>merge</sub> (%)	7.7 (30.1)	7.7 (24.8)	6.7 (29.2)	5.7 (31.1)	9.5 (25.6)	9.6 (38.0)	8.6 (38.3)
Nonhydrogen protein atoms	2270	2272	2284	2274	4538	4558	2274
Solvent molecules/ion	268/19	159/17	312/9	277/23	106/10	178/16	94/11
<i>R</i> <sub>cryst</sub> (%) / <i>R</i> <sub>free</sub> (%)	17.8/21.8	19.8/23.5	18.6/22.4	18.9/23.3	21.2/26.3	22.5/26.7	19.8/23.4
RMSD bond length (Å)	0.01	0.01	0.01	0.01	0.01	0.01	0.01
RMSD bond angle (°)	1.5	1.4	1.5	1.5	1.3	1.5	1.3
Ramachandran plot							
Most favored (%)	92.1	92.1	92.5	91.2	84.6	90.1	89.0
Additionally allowed (%)	7.9	7.5	6.6	7.5	15.1	8.8	11.0
Generously allowed (%)	0.0	0.4	0.9	1.3	0.2	1.1	0.0
Disallowed (%)	0.0	0.0	0.0	0.0	0.0	0.0	0.0
PDB code	3FJH	3FJE	3FJF	3FJJ	3FJI	3FJK	3HOM

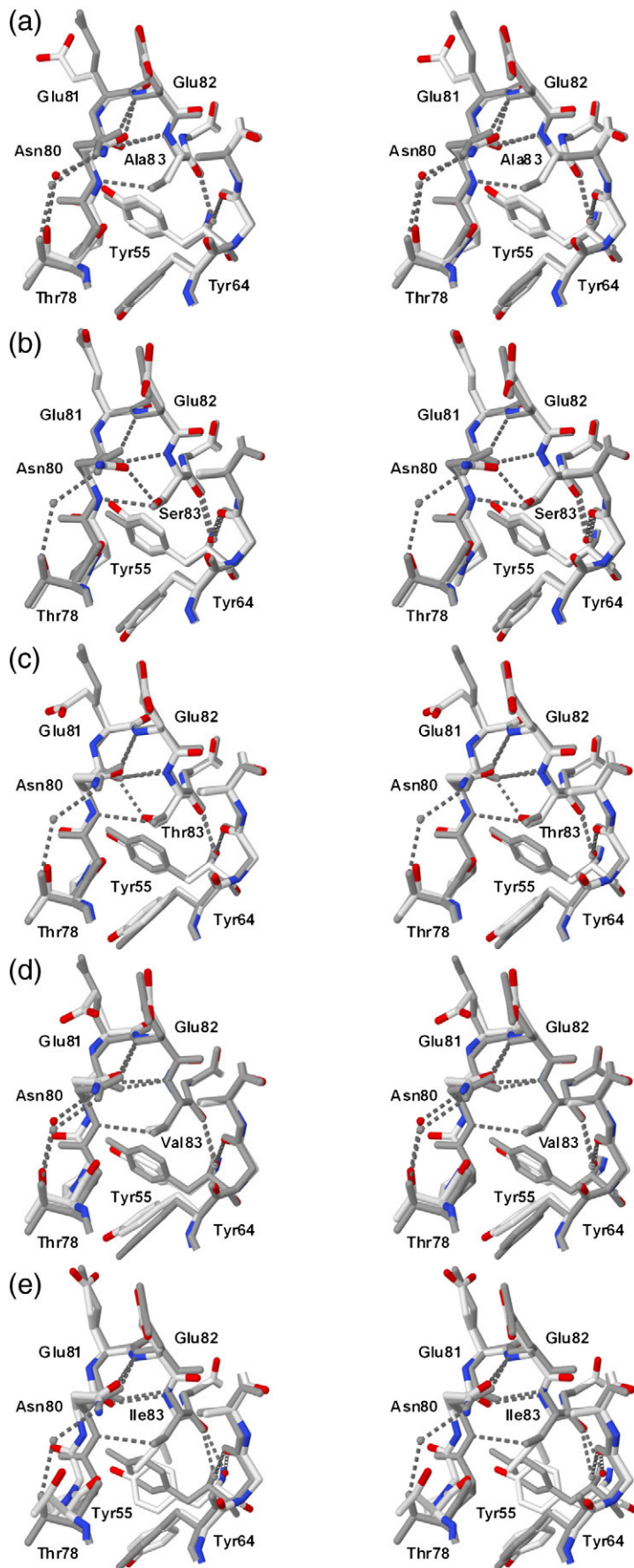


**Fig. 2.** Relaxed stereo diagram of the X-ray crystal structures (molecule A in the asymmetric unit in each case) of position 83 mutants of FGF-1 (CPK coloring) showing the structural details adjacent to the site of mutation and overlaid with the coordinates of wild-type FGF-1 (PDB code 1JQZ; light gray). (a) Cys83→Ala. (b) Cys83→Ser. (c) Cys83→Thr. (d) Cys83→Val. (e) Cys83→Ile.

O<sup>δ1</sup> acceptor; thus, the mutant Ser side chain participates in a different type of H-bond interaction in comparison to the wild-type Cys. In adjusting to position its acceptor group towards the introduced Ser, the Asn80 O<sup>δ1</sup> breaks its H-bond with the main-chain amide at position Glu82; consequently, this main-chain amide is an unsatisfied H-bond group.

#### Cys83 → Thr

The C<sup>γ2</sup> atom of the mutant Thr83 side chain juxtaposes the wild-type Cys S<sup>γ</sup> atom (Fig. 2c). In this orientation, the H-bond interaction with the main-chain amide of position Asn80 is lost, and this amide appears as an unsatisfied H-bond donor. The rotamer orientation of the mutant Thr positions the

side-chain O<sup>γ1</sup> atom adjacent to the aromatic ring of Tyr55, which moves slightly to avoid close van der Waals contact. In this orientation, the Thr O<sup>γ1</sup> introduced participates as an H-bond donor to the main-chain carbonyl group of Asn80.

#### Cys83 → Val

The mutant Val side-chain rotamer is essentially isosteric to that of the Thr83 mutant (Fig. 2d). As with the Thr83 mutant, the Asn80 main-chain amide H-bond is lost; furthermore, the novel H-bond observed with the mutant Thr83 O<sup>γ1</sup> and Asn80 main-chain carbonyl is not present. Additionally, the movement of the aromatic ring of Tyr55 appears more pronounced than with the Thr mutant.

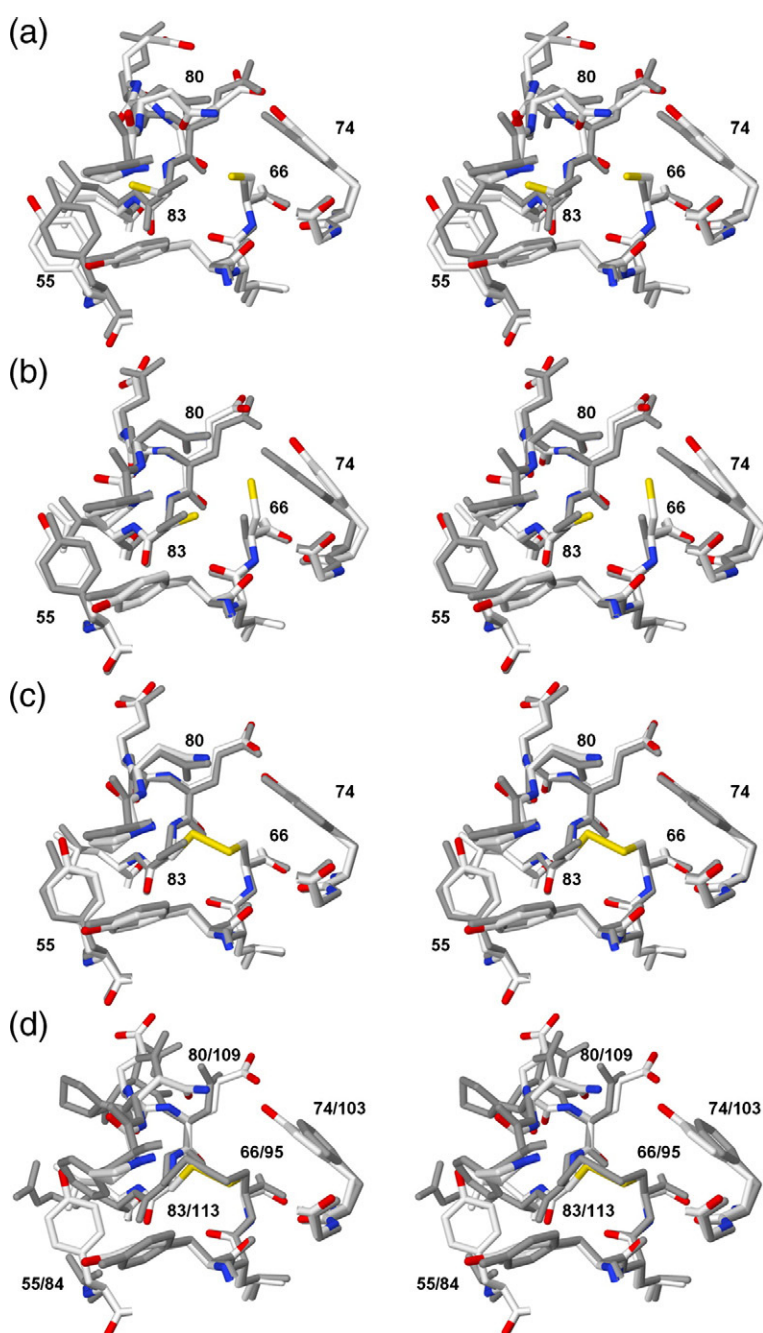


**Fig. 3.** Relaxed stereo diagram of the X-ray crystal structures of the reduced and oxidized forms of the Ala66→Cys mutant (CPK coloring). (a) Molecule A in the asymmetric unit of reduced Ala66→Cys overlaid with wild-type FGF-1 (PDB code 1JQZ; light gray). (b) Molecule B in the asymmetric unit of reduced Ala66→Cys overlaid with wild-type FGF-1 (PDB code 1JQZ; light gray). (c) Molecule A of oxidized Ala66→Cys overlaid with wild-type FGF-1 (PDB code 1JQZ; light gray). (d) Molecule A of oxidized Ala66→Cys overlaid with FGF-23 (PDB code 2P39; light gray), which contains Cys at equivalent position Cys66 in FGF-1 and forms a disulfide with Cys at equivalent position Cys83.

### Cys83→Ile

The mutant Ile side-chain C<sup>β</sup> methyl groups are not accommodated isosteric to the related Val83 mutant; rather, the Ile C<sup>γ2</sup> is oriented towards the aromatic ring of Tyr55, which rotates ~90° to avoid close van der Waals contact (Fig. 2e). With this rotamer, the mutant Ile C<sup>γ1</sup> juxtaposes with wild-type Cys83 S<sup>γ</sup>, and this positions the Ile C<sup>δ1</sup> atom between the Tyr64 aromatic ring and the C<sup>α</sup> of residue position Pro79. The C<sup>α</sup> of Pro79 shifts ~1.0 Å to accommodate the introduced Ile C<sup>δ1</sup>.

### Ala66→Cys (reduced)

The P2<sub>1</sub> crystal form has four molecules in the asymmetric unit. In molecules A and D, Cys66 adopts a *gauche+* ( $\chi_1 = -60^\circ$ ) rotamer and is oriented towards position 83; however, position 83 adopts a non-wild-type *gauche-* ( $\chi_1 = +60^\circ$ ) rotamer and is oriented away from position 66 (Fig. 3a). In response to the repositioned Cys83 S<sup>γ</sup>, the aromatic ring of adjacent Tyr55 shifts position by ~0.8 Å, and the main-chain carbonyl group of Asn80 shifts by ~1.3 Å (perturbing the local turn structure described by residue positions 79–81). Conversely, in molecules B and C, the Cys83 side chain adopts the wild-type *gauche+* ( $\chi_1 = -60^\circ$ ) rotamer and is oriented towards position 66; however, Cys66 adopts a *trans* rotamer ( $\chi_1 = 180^\circ$ ) and orients away from position 83 and towards the adjacent Tyr74 aromatic ring (Fig. 3b); in response, the Tyr74 side-chain O<sup>n</sup> shifts its position by ~1.4 Å to avoid close van der Waals contact with the Cys66 S<sup>γ</sup>. Thus, both of these alternative orientations for the Cys66 and Cys83 side chains are associated with noticeable distortion of the local structure, but principally involving the *gauche-* rotamer of Cys83 and the *trans* rotamer of Cys66. By themselves, the *gauche+* rotamers for positions Cys66 and Cys83 appear accommodated with minimal structural perturbation.

### Ala66→Cys (oxidized)

In contrast to the reduced form, the oxidized form of the Ala66→Cys mutant crystallized in the wild-type C222<sub>1</sub> space group with two molecules in the asymmetric unit. Both molecules in the asymmetric unit exhibit essentially identical structural features in the region of the Cys66 mutation and show that the introduced Cys66 forms a disulfide bond with the wild-type Cys83 residue (Fig. 3c). Each Cys residue adopts a *gauche+* rotamer in forming a disulfide bond, and the local structural features are remarkably free of any apparent perturbation. The main-chain atoms of all residues within 5.0 Å of positions 66 and 83 overlay with a root mean square deviation of 0.23 Å, essentially within the error of the X-ray data set. There is an ~0.6-Å shift of the C<sup>β</sup> of Cys83 towards Cys66 in forming the disulfide, and the aromatic ring of adjacent Tyr55 correspondingly rotates by ~0.4 Å towards Cys83.

## Discussion

Cysteine is the second least abundant amino acid in proteins (after tryptophan), yet it is among the most highly conserved in functionally important sites involving catalysis, regulation, cofactor binding, and stability.<sup>30</sup> The unique properties of cysteine have their basis in the side-chain S<sup>γ</sup> sulfur atom participating in a variety of different functional roles, including disulfide bond formation, metal binding, electron donation, hydrolysis, and redox catalysis. However, some cysteine residues do not participate in these functional roles and exist instead as structural free cysteines within the protein; these free cysteines are approximately evenly distributed between interior and solvent-exposed positions.<sup>30</sup> A relatively large body of published work has made note of the fact that free-cysteine residues within the interior of a protein can effectively limit the protein's functional half-life.<sup>27,28,31–35</sup> Such cysteines are potentially reactive thiols and subject to chemical modification should they become exposed, as transiently occurs in the dynamic equilibrium process of maintaining protein structure. Chemical modification of these cysteines can present major structural difficulties for accommodation within the native protein interior and, subsequently, typically results in an irreversible unfolding pathway. For example, if the exposed cysteine undergoes oxidation to cysteic acid, this novel ionic group is unlikely to have a countercharge appropriately positioned within the native core region. Alternatively, if the exposed cysteine forms a disulfide adduct, space must be available for this adduct within the core region; considering that most protein cores are efficiently packed, such space is unlikely to be available (especially for larger disulfide adducts involving other cysteine-containing polypeptides). Thus, in both of these examples, refolding to achieve the native structure is highly unlikely, and the unfolding process involving chemical modification of a buried thiol is considered essentially irreversible. Consequently, mutation to eliminate buried free-cysteine residues can produce a notable increase in functional half-life.<sup>27,28,30,32,36–38</sup>

The absolutely conserved Cys83 in the FGF family of proteins includes those members for which this residue participates as a half-cystine (involving the adjacent Cys66), as well as those members for which Cys83 is a buried free cysteine (and adjacent position 66 is a noncysteine residue). Thus, while Cys83 is conserved among the FGF family of proteins, there may be two distinctly different underlying roles: (1) a half-cystine, which serves to stabilize the structure, or (2) a reactive buried free cysteine, which can contribute to irreversible unfolding and thereby limit protein functional half-life. To better understand the role of the absolutely conserved Cys83 in FGF-1 (a member of the *Fgf1* subfamily where Cys83 is present as a buried free cysteine), we constructed Ala, Ser, Thr, Val, and Ile point mutations and determined the effects on stability and structure. Modeling studies suggested that only Ala,

Ser, Thr, and Val residues within this set of amino acids are able to substitute for the wild-type Cys residue without introducing unacceptably short van der Waals contacts requiring significant structural adjustment (Gly is also possible, but can introduce a main-chain entropic penalty upon stability). The Ile residue, however, was also included, since it appears conserved at the 3-fold-symmetry-related positions 42 and 130 in the  $\beta$ -trefoil structure of FGF-1.<sup>16</sup> Thermodynamic data (Table 1) show that none of the amino acids in this set can substitute for Cys83 without incurring a significant (5.2–12.6 kJ/mol) stability penalty. Furthermore, the presence of the  $\delta$ -carbon atom in the Ile side chain resulted in the greatest structural perturbation and thermodynamic destabilization of the mutations tested. Since other residue choices similarly contain a  $\delta$ -carbon atom, it is expected that they will be at least as destabilizing as the Ile residue. Thus, there is a thermodynamics-based structural preference for a Cys at position 83 in comparison to other amino acids.

The X-ray data obtained for the mutant proteins provide a structural explanation for the thermodynamic preference for a Cys at position 83 in FGF-1. Ser is isosteric with Cys and is typically considered a conservative substitution; however, the Ser oxygen atom has an approximately 0.3-Å shorter van der Waals radius than sulfur. The hydrogen bond between Cys83 and the Asn80 main-chain amide is 3.5 Å; modeling an isosteric serine into wild-type FGF-1 at position 83 results in a distance of 3.7 Å between the serine O $^{\gamma}$  and Asn80 amide. Thus, the structure must collapse by 0.3–0.4 Å to maintain this H-bond interaction with a serine mutation. If we consider first the Cys83→Ala mutation, the X-ray structure shows minimal structural collapse to fill the void left by the effective removal of the side-chain S $^{\gamma}$  and therefore indicates that the surrounding structure of position 83 is relatively rigid. The structure of the Cys83→Ser mutation indicates a similarly limited ability to collapse; the average hydrogen-bonding distance between the introduced Ser83 O $^{\gamma}$  and the Asn80 main-chain amide for the two independent molecules in the asymmetric unit is 3.7±0.4 Å, in good agreement with the modeling of a serine mutation in the wild-type structure, and shows that the Asn80 main-chain amide cannot effectively provide an H-bond donor to Ser83. The hydrogen-bonding partner that is observed in the Cys83→Ser mutant is the O $^{\delta 1}$  acceptor (2.7 Å distant) contributed by the reoriented Asn80 side chain. The Val, Thr, and Ile mutations all exhibit some degree of close van der Waals contacts with the neighboring groups, necessitating structural adjustments, and associated negative impact upon stability. X-ray data therefore indicate that the local packing environment of position 83 is both relatively rigid and optimized to accommodate a cysteine at this position in comparison to other amino acids.

In addition to the structural interactions directly involving position 83, analysis of the hydrogen-bonding details of adjacent positions shows that

these also contribute to the observed preference for cysteine at position 83. In particular, only with cysteine does the protein avoid unsatisfied H-bond interactions involving main-chain amides in the local turn structure (residues 80–83). The Asn80 main-chain amide is unsatisfied in the Cys83→Ala, Thr, Val, and Ile mutants, and the Glu82 main-chain amide is unsatisfied in the Cys83→Ala mutant, whereas both these main-chain amides are satisfied in their hydrogen-bonding requirement when cysteine is present at position 83 (see Fig. 2). Providing hydrogen-bonding partners for main-chain amides in type 1 turns is known to be important in stabilizing the turn structure;<sup>9,38–40</sup> thus, the destabilization associated with mutation of Cys83 involves the contribution of both local and more extensive hydrogen-bonding interactions.

The Ala66→Cys mutant (FGF-1 numbering scheme) tests the ability of the FGF-1 structure to accommodate a disulfide bond with the conserved Cys83. Cys66 is present in 6 of the 22 members of the FGF family, constituting two of the seven proposed archetype subfamilies: the *Fgf8* subfamily (which includes FGF-8, FGF-17, and FGF-18) and the *hFgf* subfamily (which includes FGF-19, FGF-21, and FGF-23). Among these six FGF proteins, X-ray structures are available for three: FGF-8,<sup>22</sup> FGF-19,<sup>23</sup> and FGF-23<sup>24</sup> (constituting representatives from each of the *Fgf8* and *hFgf* subfamilies), and these show a disulfide bond formed between Cys66 and Cys83.

In the crystal structure of the reduced form of the Ala66→Cys mutant, two rotamer orientations for each cysteine at positions 66 and 83, where the *gauche+* rotamer in each case is necessary for disulfide bond formation (and is the natural rotamer for the wild-type Cys83), were identified. The potential S–S distance if both cysteine rotamers are *gauche+* is 2.20 Å, optimal for forming a disulfide bond; however, the C $^{\beta}$ –S $^{\gamma}$ –S $^{\gamma}$ –C $^{\beta}$  torsion angle is  $\sim 0^{\circ}$ , where a value of  $\sim 90^{\circ}$  is canonical.<sup>41</sup> Thus, adjustments in  $\chi_1$  or the C $^{\alpha}$ –C $^{\beta}$  bond vector (via adjustment in main-chain  $\phi, \psi$  angles) for either or both residue positions 66 and 83 appear necessary to facilitate disulfide bond formation. The crystal structure of the reduced form of the Ala66→Cys mutant shows that, despite a modest instability of 5.1 kJ/mol, the native structure can stably fold with both Cys66 and Cys83 in the reduced state and, in doing so, bring these potentially reactive thiols adjacent to each other; furthermore, X-ray data show that both the Cys66 side chain and the Cys83 side chain sample the specific rotamer orientations (*gauche+*) necessary to form a disulfide bond.

The X-ray structure of the oxidized form of the Ala66→Cys mutant shows formation of a disulfide bond between residues Cys66 and Cys83 (both molecules in the asymmetric unit are essentially identical in this regard). The resulting C $^{\beta}$ –S $^{\gamma}$ –S $^{\gamma}$ –C $^{\beta}$  torsion angle is observed to be a canonical  $90^{\circ}$ , accomplished principally through a C $^{\alpha}$ –C $^{\beta}$  vector adjustment involving position 83; other than this, the structural perturbation in response to the introduction of the disulfide bond is negligible. Thus, the

wild-type FGF-1 structure readily accommodates the Ala66→Cys mutant in a rotamer that favors disulfide bond formation with adjacent Cys83, and Cys83 in the wild-type structure appears appropriately positioned (and also potentially deprotonated) to form a disulfide bond with an introduced Cys66.

Under reducing conditions, the Ala66→Cys mutant in FGF-1 is 5.1 kJ/mol less stable than the wild-type protein (Table 1), and X-ray data show perturbation of the local structure with both of the alternative conformations observed for the pair of free cysteines at positions 66 and 83 (Fig. 3a and b). In contrast, the Cys83→Ala mutation in wild-type FGF-1 is 5.7 kJ/mol destabilizing; thus, while position 83 in the wild-type protein is optimized to accept a Cys residue, position 66 is not. Nonetheless, the Ala66→Cys mutant yields a substantial gain in stability upon oxidation to form a disulfide bond with adjacent Cys83, indicating that the wild-type FGF-1 structure is predisposed to accommodating a favorable disulfide bond between positions 66 and 83 and that any strain introduced by forming a disulfide is more than offset by the entropically based gain in stability.<sup>42</sup>

FGF-23 (PDB code 2P39) is an example of one of the six FGF family members with a cysteine residue at a position equivalent to Ala66 in the wild-type FGF-1 sequence and whose crystal structure shows formation of a disulfide bond with the equivalent Cys83.<sup>24</sup> An overlay of the oxidized Ala66→Cys mutant X-ray structure with that of FGF-23 shows an essentially identical disulfide bond arrangement (Fig. 3d). However, we note that in each of the structures of the *Fgf* members with a disulfide bond involving positions 66 and 83, there is an amino acid insertion in the adjacent loop 80–83 region. This insertion may permit a small but important structural adjustment that promotes a more optimal stereochemistry for disulfide bond formation between Cys66 and Cys83.

A disulfide bond between Cys66 and Cys83 is present in two of the seven archetype subfamilies (*Fgf8* and *hFgf*) produced after the hypothesized first expansion of the *Fgf* family from one or several members. Thus, this cystine either emerged independently in two different members after this expansion or existed prior to this expansion and is a truly ancient structural feature of the *Fgf* family. The current results suggest that the free-cysteine residue at position 83 in FGF-1 represents one-half of an archetype cystine involving position 66. In this hypothesis, the disulfide has been lost due to mutation of position 66, but can nonetheless be recovered by “backmutation” of position 66 to cysteine. Wild-type FGF-1 is less stable with the loss of this disulfide; however, the low thermal stability of FGF-1 and FGF-2 may be essential to their nontraditional secretion mechanism.<sup>43–45</sup> Additionally, as a potent mitogen, limiting functional half-life may be important; elimination of reactive thiols in FGF-1 (despite being significantly destabilizing) has been shown to increase the protein

functional half-life by 2 orders of magnitude<sup>26–28</sup>. The *hFgf* family members (which contain a position 66/83 cystine) are unique in that they function in an endocrine fashion distal to the cells that secrete them; in this case, enhanced stability (as well as increased functional half-life) may be more important. Thus, while Cys83 is absolutely conserved in the *Fgf* family, the underlying basis for its retention may vary between family members and involve differential concerns of stability and regulation of functional half-life. The results with FGF-1 suggest that other members of the *Fgf* family with a free cysteine at position 83 may similarly be stabilized by the introduction of a novel disulfide bond involving a cysteine at position 66, with an associated favorable impact on functional half-life due to both increased thermostability and effective elimination of a buried free thiol.

## Materials and Methods

### Mutagenesis and expression

All studies utilized a synthetic gene for the 140-amino acid form of human FGF-1<sup>15,16,46,47</sup> containing an additional amino-terminal His tag, as previously described.<sup>12</sup> The QuikChange™ site-directed mutagenesis protocol (Stratagene, La Jolla, CA) was used to introduce all point mutations, which were confirmed by nucleic acid sequence analysis (Biomolecular Analysis Synthesis and Sequencing Laboratory, Florida State University). All expression and purification protocols followed previously published procedures.<sup>12</sup> Purified protein was exchanged into 50 mM sodium phosphate, 0.1 M NaCl, 10 mM ammonium sulfate, and 2 mM DTT (pH 7.5) (“crystallization buffer”). Due to the potential for disulfide bond formation, the purified Ala66→Cys mutant protein was exchanged against crystallization buffer both with and without the inclusion of DTT. The yield for most of the mutant proteins was 20–40 mg/L; however, Cys83→Ile could not be isolated due to significant precipitation during purification (suggesting substantial destabilization). Therefore, Cys83→Ile was constructed in a Lys12→Val/Cys117→Val stabilizing background.<sup>29</sup> Lys12→Val/Cys117→Val was chosen since these mutation sites are distal to position Cys83 while providing –8.1 kJ/mol of additional thermostability.

### Isothermal equilibration denaturation

This method makes use of the fluorescence signal of the single endogenous Trp residue at position 107 in FGF-1; this residue is ~90% buried in the native structure<sup>16</sup> and is therefore useful as a spectroscopic probe of protein denaturation. Complete details of the instrumentation, data collection, and analysis procedure have been previously reported.<sup>48</sup> Briefly, the fluorescence signal of FGF-1 is atypical in that Trp107 exhibits greater quenching in the native state than in the denatured state. Excitation at 295 nm provides selective excitation of Trp107 in comparison with the six Tyr residues that are present in the structure.<sup>12,48</sup> Protein samples (5 μM) in various concentrations of guanidine hydrochloride were allowed to equilibrate overnight at room temperature (298 K). Triplicate scans were collected and averaged, and buffer

traces were collected and subsequently subtracted from protein scans. All scans were integrated to quantify the total fluorescence as a function of denaturant concentration. The data were analyzed using a general-purpose nonlinear least-squares fitting program (DataFit; Oakdale Engineering, Oakdale, PA) implementing a six-parameter two-state model:<sup>49</sup>

$$F \frac{F_{0N} + S_N[D] + (F_{0D} + (S_D[D]))e^{-(\Delta G_0 + m[D])/RT}}{1 + e^{-(\Delta G_0 + m[D])/RT}} \quad (1)$$

where [D] is the denaturant concentration;  $F_{0N}$  and  $F_{0D}$  are the 0 M denaturant intercepts for the native-state and denatured-state baselines, respectively; and  $S_N$  and  $S_D$  are the slopes of the native-state and denatured-state baselines, respectively.  $\Delta G_0$  and  $m$  describe the linear function of the unfolding free energy *versus* denaturant concentration. The effect of a given mutation on the stability of the protein ( $\Delta\Delta G$ ) was calculated by taking the difference between the  $C_m$  value for wild-type protein and the  $C_m$  value for mutant protein and multiplying by the average of the  $m$  values, as described by Pace and Scholtz:<sup>50</sup>

$$\Delta\Delta G = (C_m \text{ WT} - C_m \text{ mutant})(m_{\text{WT}} + m_{\text{mutant}})/2 \quad (2)$$

where a negative value indicates that the mutation is stabilizing in relationship to the wild-type protein.

### Mass spectrometry

Ala66→Cys mutant protein, purified either in the presence or in the absence of 10 mM DTT, was digested with trypsin (200:1 molar ratio, respectively; Sigma Chemical Co., St. Louis, MO) for 3 h at 37 °C. Cleaved peptide fragments were subjected to matrix-assisted laser desorption ionization time-of-flight mass spectrometry analysis on a model 4700 Proteomics Analyzer (Applied Biosystems, Foster City, CA) using a matrix of  $\alpha$ -cyano 4-hydroxy cinnamic acid (5 mg/ml in 50% acetonitrile and 0.1% trifluoroacetic acid). A six-point mass standard kit (Applied Biosystems) was used to perform external calibration for each spectrum and to permit a mass accuracy of within 20 ppm. The 31-amino-acid peptide fragment STETGQYLMDTDGLLYGSQTPNEECLFLER (residue positions 58–88 of FGF-1) generated by trypsin digest contains both Cys66 and Cys83 residues. The combined oxidative state of these Cys residues was evaluated by the mass of this fragment.

### Crystallization, data collection, molecular replacement, and refinement

Purified mutant protein in crystallization buffer was concentrated to 9–13 mg/ml, and crystals were grown using the hanging-drop vapor diffusion method. Crystals suitable for diffraction grew in 1 week at room temperature with 1 ml of reservoir solution containing 2.0–3.5 M sodium formate and 0.1–1.0 M ammonium sulfate in the crystallization buffer. The Ala66→Cys mutant crystal setups were performed using protein purified in the presence of 10 mM DTT (“reduced A66C”), as well as protein purified in the absence of DTT, and subsequently air oxidized for 3 weeks prior to crystallization trials (“oxidized A66C”). The crystallization buffer for the oxidized A66C protein was prepared, omitting DTT. Diffraction data for all mutant proteins, except for Cys83→Ile/Lys12→Val/Cys117→Val, were collected

using an in-house Rigaku RU-H2R rotating-anode X-ray source (Rigaku MSC, The Woodlands, TX) equipped with Osmic Blue confocal mirrors (MarUSA, Evanston, IL) and a Rigaku R-axis IIc image plate detector. Diffraction of the Cys83→Ile/Lys12→Val/Cys117→Val mutation was performed at the Southeast Regional Collaborative Access Team 22-BM beamline ( $\lambda = 1.00 \text{ \AA}$ ) at the Advanced Photon Source at the Argonne National Laboratory using a MarCCD 225 detector (MarUSA). Crystals were mounted using Hampton Research (Aliso Viejo, CA) nylon-mounted cryoturns and frozen in a stream of nitrogen gas at 100 K. Diffraction data were indexed, integrated, and scaled using the DENZO software package.<sup>51,52</sup> His-tagged wild-type FGF-1 (PDB code 1JQZ) was used as search model in molecular replacement for all structures using the CNS software.<sup>53</sup> Model building and visualization utilized either the O program or the Coot molecular graphics software.<sup>54,55</sup> Structure refinement utilized either the CNS or the PHENIX software,<sup>53,56</sup> with 5% of the data in the reflection files set aside for  $R_{\text{free}}$  calculations.<sup>57</sup> Quantification of solvent-excluded cavities with the refined mutant structures was performed using the Molecular Surface Package software.<sup>58</sup>

### Accession numbers

Coordinates and structure factors have been deposited in the PDB with accession numbers 3FJH, 3FJE, 3FJF, 3FJJ, 3FJI, 3FJK, and 3HOM.

### Acknowledgements

We thank Dr. T. Somasundaram (X-ray Crystallography Facility) and Dr. Claudius Mundoma (Physical Biochemistry Facility, Kasha Laboratory, Institute of Molecular Biophysics) for valuable suggestions and technical assistance. We also thank Ms. Pushparani Dhanarajan (Molecular Cloning Facility, Department of Biological Science) for helpful comments. We acknowledge the instrumentation facilities of the Biomedical Proteomics Laboratory, College of Medicine. This work was supported by grant 0655133B from the American Heart Association. The use of the “mail-in crystallography” facility of the Southeast Regional Collaborative Access Team for diffraction data collection is acknowledged. The use of the Advanced Photon Source was supported by the US Department of Energy, Basic Energy Sciences, Office of Science, under contract no. W-31-109-Eng-38. All X-ray structures have been deposited in the PDB.

### References

1. Itoh, N. & Ornitz, D. M. (2004). Evolution of the *Fgf* and *Fgfr* gene families. *Trends Genet.* **20**, 563–569.
2. Popovici, C., Roubin, R., Coulier, F. & Birnbaum, D. (2005). An evolutionary history of the FGF superfamily. *BioEssays*, **27**, 849–857.
3. Holland, P. W. H., Garcia-Fernandez, J., Williams, N. A. & Sidow, A. (1994). Gene duplications and the origins of vertebrate development. *Dev. Suppl.* 125–133.

4. Itoh, N. & Ornitz, D. M. (2008). Functional evolutionary history of the mouse *Fgf* gene family. *Dev. Dyn.* **237**, 18–27.
5. Murzin, A. G., Lesk, A. M. & Chothia, C. (1992).  $\beta$ -Trefoil fold. Patterns of structure and sequence in the Kunitz inhibitors interleukins-1 $\beta$  and 1 $\alpha$  and fibroblast growth factors. *J. Mol. Biol.* **223**, 531–543.
6. Hutchinson, E. G. & Thornton, J. M. (1994). A revised set of potentials for beta-turn formation in proteins. *Protein Sci.* **3**, 2207–2216.
7. Guruprasad, K. & Rajkumar, S. (2000). Beta- and gamma-turns in proteins revisited: a new set of amino acid turn-type dependent positional preferences and potentials. *J. Biosci.* **25**, 143–156.
8. Kim, J., Brych, S. R., Lee, J., Logan, T. M. & Blaber, M. (2003). Identification of a key structural element for protein folding within  $\beta$ -hairpin turns. *J. Mol. Biol.* **328**, 951–961.
9. Lee, J., Dubey, V. K., Longo, L. M. & Blaber, M. (2008). A logical OR redundancy with the Asx-Pro-Asx-Gly type I  $\beta$ -turn motif. *J. Mol. Biol.* **377**, 1251–1264.
10. Shortle, D., Stites, W. E. & Meeker, A. K. (1990). Contributions of the large hydrophobic amino acids to the stability of staphylococcal nuclease. *Biochemistry*, **29**, 8033–8041.
11. Eriksson, A. E., Baase, W. A., Zhang, X.-J., Heinz, D. W., Blaber, M., Baldwin, E. P. & Matthews, B. W. (1992). Response of a protein structure to cavity-creating mutations and its relation to the hydrophobic effect. *Science*, **255**, 178–183.
12. Brych, S. R., Blaber, S. I., Logan, T. M. & Blaber, M. (2001). Structure and stability effects of mutations designed to increase the primary sequence symmetry within the core region of a  $\beta$ -trefoil. *Protein Sci.* **10**, 2587–2599.
13. Burgess, W., Mehlman, T., Freisel, R., Johnson, W. & Maciag, T. (1985). Multiple forms of endothelial cell growth factor: rapid isolation and biological and chemical characterization. *J. Biol. Chem.* **260**, 11389–11392.
14. Strydom, D., Harper, J. W. & Lobb, R. (1986). Amino acid sequence of bovine brain-derived class 1 heparin-binding growth factor. *Biochemistry*, **25**, 945–951.
15. Linemeyer, D. L., Menke, J. G., Kelly, L. J., DiSalvo, J., Soderman, D., Schaeffer, M.-T. *et al.* (1990). Disulfide bonds are neither required, present, nor compatible with full activity of human recombinant acidic fibroblast growth factor. *Growth Factors*, **3**, 287–298.
16. Blaber, M., DiSalvo, J. & Thomas, K. A. (1996). X-ray crystal structure of human acidic fibroblast growth factor. *Biochemistry*, **35**, 2086–2094.
17. Zhang, J., Cousens, L. S., Barr, P. J. & Sprang, S. R. (1991). Three-dimensional structure of human basic fibroblast growth factor, a structural homolog of interleukin 1B. *Proc. Natl Acad. Sci. USA*, **88**, 3446–3450.
18. Bellosta, P., Iwahori, A., Plotnikov, A. N., Eliseenkova, A. V., Basilico, C. & Mohammadi, M. (2001). Identification of receptor and heparin binding sites in fibroblast growth factor 4 by structure-based mutagenesis. *Mol. Cell. Biol.* **21**, 5946–5957.
19. Ye, S., Luo, Y., Jones, R. B., Linhardt, R. J., Capila, I., Toida, T. *et al.* (2001). Structural basis for interaction of FGF-1, FGF-2, and FGF-7 with different heparan sulfate motifs. *Biochemistry*, **40**, 14429–14439.
20. Plotnikov, A. N., Eliseenkova, A. V., Ibrahim, O. A., Shriver, Z., Sasisekharan, R., Lemmon, M. A. & Mohammadi, M. (2001). Crystal structure of fibroblast growth factor 9 reveals regions implicated in dimerization and autoinhibition. *J. Biol. Chem.* **276**, 4322–4329.
21. Yeh, B. K., Igarashi, M., Eliseenkova, A. V., Plotnikov, A. N., Sher, L., Ron, D. *et al.* (2003). Structural basis by which alternative splicing confers specificity in fibroblast growth factor receptors. *Proc. Natl Acad. Sci. USA*, **100**, 2266–2271.
22. Olsen, S. K., Li, J. Y. H., Bromleigh, C., Eliseenkova, A. V., Ibrahim, O. A., Lao, Z. *et al.* (2006). Structural basis by which alternative splicing modulates the organizer activity of FGF8 in the brain. *Genes Dev.* **20**, 185–198.
23. Harmer, N. J., Pellegrini, L., Chirgadze, D., Fernandez-Recio, J. & Blundell, T. L. (2004). The crystal structure of fibroblast growth factor (FGF) 19 reveals novel features of the FGF family and offers a structural basis for its unusual receptor affinity. *Biochemistry*, **43**, 629–640.
24. Goetz, R., Beenken, A., Ibrahim, O. A., Kalinina, J., Olsen, S. K., Eliseenkova, A. V. *et al.* (2007). Molecular insights into the klotho-dependent, endocrine mode of action of fibroblast growth factor 19 subfamily members. *Mol. Cell Biol.* **27**, 3417–3428.
25. Itoh, N. (2007). The FGF families in humans, mice, zebrafish: their evolutionary processes and roles in development, metabolism, and disease. *Biol. Pharm. Bull.* **30**, 1819–1825.
26. Culajay, J. F., Blaber, S. I., Khurana, A. & Blaber, M. (2000). Thermodynamic characterization of mutants of human fibroblast growth factor 1 with an increased physiological half-life. *Biochemistry*, **39**, 7153–7158.
27. Ortega, S., Schaeffer, M.-T., Soderman, D., DiSalvo, J., Linemeyer, D. L., Gimenez-Gallego, G. & Thomas, K. A. (1991). Conversion of cysteine to serine residues alters the activity, stability, and heparin dependence of acidic fibroblast growth factor. *J. Biol. Chem.* **266**, 5842–5846.
28. Lee, J. & Blaber, M. (2009). The interaction between thermodynamic stability and buried free cysteines in regulating the functional half-life of fibroblast growth factor-1. *J. Mol. Biol.* **393**, 113–127.
29. Dubey, V. K., Lee, J., Somasundaram, T., Blaber, S. & Blaber, M. (2007). Spackling the crack: stabilizing human fibroblast growth factor-1 by targeting the N and C terminus beta-strand interactions. *J. Mol. Biol.* **371**, 256–268.
30. Fomenko, D. E., Marino, S. M. & Gladyshev, V. N. (2008). Functional diversity of cysteine residues in proteins and unique features of catalytic redox-active cysteines in thiol oxidoreductases. *Mol. Cells*, **26**, 228–235.
31. Petersen, M. T. N., Jonson, P. H. & Petersen, S. B. (1999). Amino acid neighbours and detailed conformational analysis of cysteines in proteins. *Protein Eng.* **12**, 535–548.
32. Perry, L. J. & Wetzel, R. (1987). The role of cysteine oxidation in the thermal inactivation of T4 lysozyme. *Protein Eng.* **1**, 101–105.
33. McRee, D. E., Redford, S. M., Getzoff, E. D., Lepock, J. R., Hallewell, R. A. & Tainer, J. A. (1990). Changes in crystallographic structure and thermostability of a Cu,Zn superoxide dismutase mutant resulting from the removal of a buried cysteine. *J. Biol. Chem.* **265**, 14234–14241.
34. Faletto, M. B., Linko, P. & Goldstein, J. A. (1992). A single amino acid mutation (Ser180-Cys) determines the polymorphism in cytochrome P450g (P450C13) by altering protein stability. *J. Biol. Chem.* **267**, 2032–2037.
35. Fremaux, I., Mazeres, S., Brisson-Lougarre, A., Arnaud, M., Ladurantie, C. & Fournier, D. (2002). Improvement

- of *Drosophila* acetylcholinesterase stability by elimination of a free cysteine. *BMC Biochem.* **3**, 21.
36. Engleka, K. A. & Maciag, T. (1992). Inactivation of human fibroblast growth factor-1 (FGF-1) activity by interaction with copper ions involves FGF-1 dimer formation induced by copper-catalyzed oxidation. *J. Biol. Chem.* **267**, 11307–11315.
  37. Estape, D., van den Heuvel, J. & Rinas, U. (1998). Susceptibility towards intramolecular disulphide-bond formation affects conformational stability and folding of human basic fibroblast growth factor. *Biochem. J.* **335**, 343–349.
  38. Santiveri, C. M., Jimenez, M. A., Rico, M., Van Gunsteren, W. F. & Daura, X. (2004). Beta-hairpin folding and stability: molecular dynamics simulations of designed peptides in aqueous solution. *J. Pept. Sci.* **10**, 546–565.
  39. de Alba, E., Jimenez, M. A. & Rico, M. (1997). Turn residue sequence determines beta-hairpin conformation in designed peptides. *J. Am. Chem. Soc.* **119**, 175–183.
  40. Wan, W.-Y. & Milner-White, E. J. (1999). A natural grouping of motifs with an aspartate or asparagine residue forming two hydrogen bonds to residues ahead in sequence: their occurrence at  $\alpha$ -helical N termini and in other situations. *J. Mol. Biol.* **286**, 1633–1649.
  41. Bhattacharyya, R., Pal, D. & Chakrabarti, P. (2004). Disulfide bonds, their stereospecific environment and conservation in protein structures. *Protein Eng. Des. Sel.* **17**, 795–808.
  42. Matsumura, M., Becktel, W. J., Levitt, M. & Matthews, B. W. (1989). Stabilization of phage T4 lysozyme by engineered disulfide bonds. *Proc. Natl Acad. Sci. USA*, **86**, 6562–6566.
  43. Florkiewicz, R. Z., Majack, R. A., Buechler, R. D. & Florkiewicz, E. (1995). Quantitative export of FGF-2 occurs through an alternative, energy-dependent, non-ER/Golgi pathway. *J. Cell. Physiol.* **162**, 388–399.
  44. Jackson, A., Friedman, S., Zhan, X., Engleka, K. A., Forough, R. & Maciag, T. (1992). Heat shock induces the release of fibroblast growth factor 1 from NIH 3T3 cells. *Proc. Natl Acad. Sci. USA*, **89**, 10691–10695.
  45. Mach, H. & Middaugh, C. R. (1995). Interaction of partially structured states of acidic fibroblast growth factor with phospholipid membranes. *Biochemistry*, **34**, 9913–9920.
  46. Gimenez-Gallego, G., Conn, G., Hatcher, V. B. & Thomas, K. A. (1986). The complete amino acid sequence of human brain-derived acidic fibroblast growth factor. *Biochem. Biophys. Res. Commun.* **128**, 611–617.
  47. Cuevas, P., Carceller, F., Ortega, S., Zazo, M., Nieto, I. & Gimenez-Gallego, G. (1991). Hypotensive activity of fibroblast growth factor. *Science*, **254**, 1208–1210.
  48. Blaber, S. I., Culajay, J. F., Khurana, A. & Blaber, M. (1999). Reversible thermal denaturation of human FGF-1 induced by low concentrations of guanidine hydrochloride. *Biophys. J.* **77**, 470–477.
  49. Eftink, M. R. (1994). The use of fluorescence methods to monitor unfolding transitions in proteins. *Biophys. J.* **66**, 482–501.
  50. Pace, C. N. & Scholtz, J. M. (1997). Measuring the conformational stability of a protein. In *Protein Structure: A Practical Approach* (Creighton, T. E., ed), pp. 299–321, Oxford University Press, Oxford.
  51. Otwinowski, Z. (1993). In *Proceedings of the CCP4 Study Weekend: Data Collection and Processing* (Sawyer, L., Isaacs, N. & Bailey, S., eds), pp. 55–62, SERC Daresbury Laboratory, Warrington, UK.
  52. Otwinowski, Z. & Minor, W. (1997). Processing of X-ray diffraction data collected in oscillation mode. *Methods Enzymol.* **276**, 307–326.
  53. Brunger, A. T., Adams, P. D., Clore, G. M., DeLano, W. L., Gros, P., Grosse-Kunstleve, R. W. *et al.* (1998). Crystallography and NMR system (CNS): a new software system for macromolecular structure determination. *Acta Crystallogr. Sect. D*, **54**, 905–921.
  54. Johnson, D. E., Lu, J., Chen, H., Werner, S. & Williams, L. T. (1991). The human fibroblast growth factor receptor genes: a common structural arrangement underlies the mechanisms for generating receptor forms that differ in their third immunoglobulin domain. *Mol. Cell. Biol.* **11**, 4627–4634.
  55. Emsley, P. & Cowtan, K. (2004). Coot: model-building tools for molecular graphics. *Acta Crystallogr. Sect. D*, **60**, 2126–2132.
  56. Zwart, P. H., Afonine, P. V., Grosse-Kunstleve, R. W., Hung, L. W., Loerger, T. R., McCoy, A. J. *et al.* (2008). Automated structure solution with the PHENIX suite. *Methods Mol. Biol.* **426**, 419–435.
  57. Brunger, A. T. (1992). Free *R* value: a novel statistical quantity for assessing the accuracy of crystal structures. *Nature*, **355**, 472–475.
  58. Connolly, M. L. (1993). The Molecular Surface Package. *J. Mol. Graphics*, **11**, 139–141.